DOI: 10.1002/ejic.200601029

Controlled Synthesis and Characterization of CuO Nanostructures through a Facile Hydrothermal Route in the Presence of Sodium Citrate

Hong-Mei Xiao,[a,b] Shao-Yun Fu,*[a] Lu-Ping Zhu,[a,b] Yuan-Qing Li,[a,b] and Guo Yang[a,b]

Keywords: Hydrothermal synthesis / Nanostructures / Sodium citrate / Copper complexes

The controlled synthesis of one-dimensional, two dimensional, and three-dimensional CuO nanostructures has been achieved by a hydrothermal process in the presence of sodium citrate (SC) by simply controlling the reaction conditions. When the molar ratio of sodium citrate to $CuSO_4 \cdot 5H_2O$ (represented by SC/Cu^{2+}) is below 1.0, 1D CuO nanorods with 30–40 nm diameters and 100–200 nm lengths are formed. In the absence of citrate, 2D flakelike CuO nanostructures with 150–200 nm widths and 300–400 nm lengths are obtained. When the SC/Cu^{2+} ratio is more than 1.0, 3D branchlike CuO nanostructures with lengths of hundreds of nanometers and diameters of 20–100 nm are attained. On the basis of the morphology and X-ray diffraction patterns of the samples, a possible growth mechanism for the CuO nanostructures is proposed. Moreover, it is shown that the optical bandgap energy (E_g) of resulting CuO nanostructures can be tuned through morphological control of the CuO nanostructures. Ultraviolet absorption measurements reveal that the estimated bandgap energy of the 1D rodlike, 2D flakelike, and 3D branchlike CuO nanostructures is 2.36, 1.60, and 1.40 eV, respectively.

Introduction

Copper monoxide based materials are well known because of their relevance in high-temperature superconductivity and semiconducting antiferromagnetism.[1] CuO is a narrow bandgap (E_g = 1.2 eV) *p*-type semiconductor and has been recognized as an industrially important material for a variety of practical applications, such as catalysis, solar energy conversion, gas sensing and field emission, in batteries, and in magnetic storage media.[2–14] Nanosized CuO may exhibit unique properties that can be significantly different from those of their bulk counterparts, for example, unusual optical, electrical, and catalytic properties, etc.[15a] Therefore, the synthesis and study of CuO nanostructures is both of practical and fundamental importance. In the last two decades, great efforts have been made to synthesize CuO nanostructures with various morphologies by a variety of wet chemical methods.[15–27] Among the various methods developed for fabrication of nanostructured CuO materials, the hydrothermal process has been considered as the most promising route because it is simple and can operate at low-temperatures and in a large scale.[16,19]

Besides the great interest in synthetic methods of the CuO nanostructures, there is a growing interest in the morphological control of CuO nanostructures.[18a,18d,28,29] Wet chemical methods, in which a water/ethanol mixture was used, were reported for the controlled synthesis of 1D CuO nanostructures, namely nanorods and nanoribbons, by controlling reagent concentrations.[18a] Controlled synthesis of CuO nanostructures such as nanoplatelets, nanoleaflets and nanowires was also realized by thermal dehydration of the as-prepared $Cu(OH)_2$ nanostructures in solution or in the solid state.[18d] CuO nanosheets and nanowhiskers were successfully obtained by controlling the liquid–solid reaction on copper surfaces under alkaline and oxidative conditions.[28] As mentioned above, the hydrothermal method is advantageous as it is simple and can operate at low temperatures and in a large scale, and hence should be more promising route for the controlled synthesis of CuO nanostructures, but this has not been reported previously.

It was claimed that semiconductors with bandgap energies in the range from 1 to 3 eV have important applications in solid-state photonic devices.[30] Various CuO nanostructures with different bandgap energies were reported.[15d,27b,29,31] A bandgap of 2.1 eV was reported for CuO nanoparticles,[15d] 2.78 eV for needle-shaped CuO nanocrystals,[31] 3.02 eV for CuO nanoplatelets,[27b] and 2.05 and 2.47 eV for CuO nanoellipsoids and nanosheets, respectively.[29] Moreover, the bandgap energy of CuO nanofibrils was estimated to be 1.67 eV.[32] Obviously, the bandgap energy depends on the morphology of CuO nanostructures. Thus, it can be expected that the bandgap energy of CuO nanostructures can be tuned by controlling the morphology of CuO nanostructures.

[a] Technical Institute of Physics and Chemistry, Chinese Academy of Sciences,
Beijing 100080, China
Fax: +86-10-82543752
E-mail: syfu@cl.cryo.ac.cn
syfu@mail.ipc.ac.cn
[b] Graduate School, Chinese Academy of Sciences,
Beijing 100039, P. R. China

It is well known that sodium citrate (SC) is an important biological ligand for metal ions. It has been widely employed as a reductant and capping agent in the synthesis of elemental Ag, Au, and Ag–Au alloy nanoparticles.[33] It also serves as shape controller and stabilizer in the synthesis of $Ni(OH)_2$, calcite, coated CdSe colloids, doughnut-shaped ZnO microparticles, calcium phosphate and CuI crystals.[34] In this study, sodium citrate was employed for the first time for the controllable synthesis of CuO nanostructures with various morphologies using the hydrothermal process.

The controlled synthesis of nanostructured CuO samples with various morphologies was realized using the facile hydrothermal process through changing the molar ratio of sodium citrate to $CuSO_4 \cdot 5H_2O$ only. On the basis of the morphology and X- ray diffraction patterns of the samples, a possible growth mechanism for the CuO nanostructures was proposed. Moreover, UV absorption measurements show that CuO nanostructures display a blue shift of the bandgap relative to bulk CuO material and that the bandgap energy of the CuO nanostructures is tunable by controlling the morphology of the CuO nanostructures.

Results and Discussion

The Role of SC on Crystal Structure and Morphology

The control of the phase of the products through the hydrothermal route is shown in Figure 1. Figure 1a presents the XRD pattern of the product obtained without the addition of sodium citrate, and all peaks in the XRD patterns of the sample are consistent with the JCPDS (5–0661) data of copper oxide with a monoclinic phase.[35] When the SC/Cu^{2+} ratio is 1.0, the XRD diffraction peaks can be indexed as the monoclinic phase of CuO (Figure 1b). The atomic ratio of Cu to O was estimated to be 1:1 by SEM-EDS elemental analysis (inset in Figure 1). However, when the SC/Cu^{2+} is increased to 1.3, the XRD pattern of the obtained sample shows that the sample is no longer pure monoclinic CuO – a weak peak of cubic Cu_2O also appears (Figure 1c). The above results indicate that citrate is very important in controlling the phase of the products during the hydrothermal process.

The influence of sodium citrate on the morphology of the CuO products was examined by scanning electron microscopy (SEM) and transmission electron microscopy (TEM). Figure 2a,b shows that the 2D flakelike CuO nanostructures with a width of 150–200 nm and a length of 300–400 nm were obtained by the hydrothermal process without citrate. Moreover, the 1D CuO nanorods with diameters of 30–40 nm and lengths of 100–120 nm were formed when the SC/Cu^{2+} ratio was 1.0, as shown in Figure 2c,d. Figure 2e,f shows the 3D branchlike CuO nanostructures at a SC/Cu^{2+} ratio of 1.3. The branchlike CuO nanostructures consist of sub-branched nanorods with diameters of about 20–100 nm, which radiate from the sides of the main stem of the branchlike CuO nanostructures.

The electron diffraction (ED) patterns of 1D (inset in Figure 2d), 2D (inset in Figure 2b), and 3D (inset in Figure 2f) CuO show that they are all single crystals.

Formation Mechanism

Figure 3a shows the molecular structure of sodium citrate with three carbonyl groups and one hydroxy group. After the addition of sodium citrate to $CuSO_4 \cdot 5H_2O$, Cu^{2+} and sodium citrate form a complex. Daniele et al. reported that the main component of citrate solutions of Cu^{2+} in the

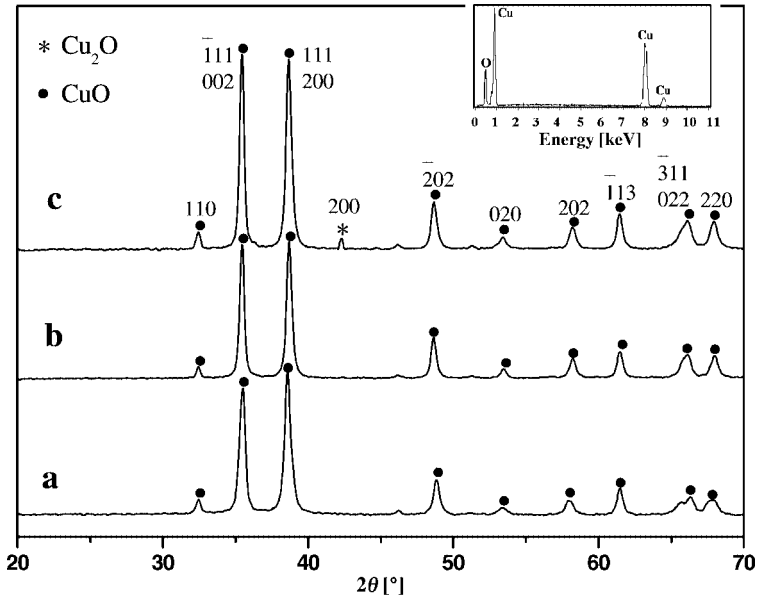

Figure 1. XRD patterns of the samples prepared by the hydrothermal route: (a) without sodium citrate, (b) SC/Cu^{2+} = 1.0, and (c) SC/Cu^{2+} = 1.3. The inset presents the SEM-EDS elemental analysis of the sample with SC/Cu^{2+} = 1.0.

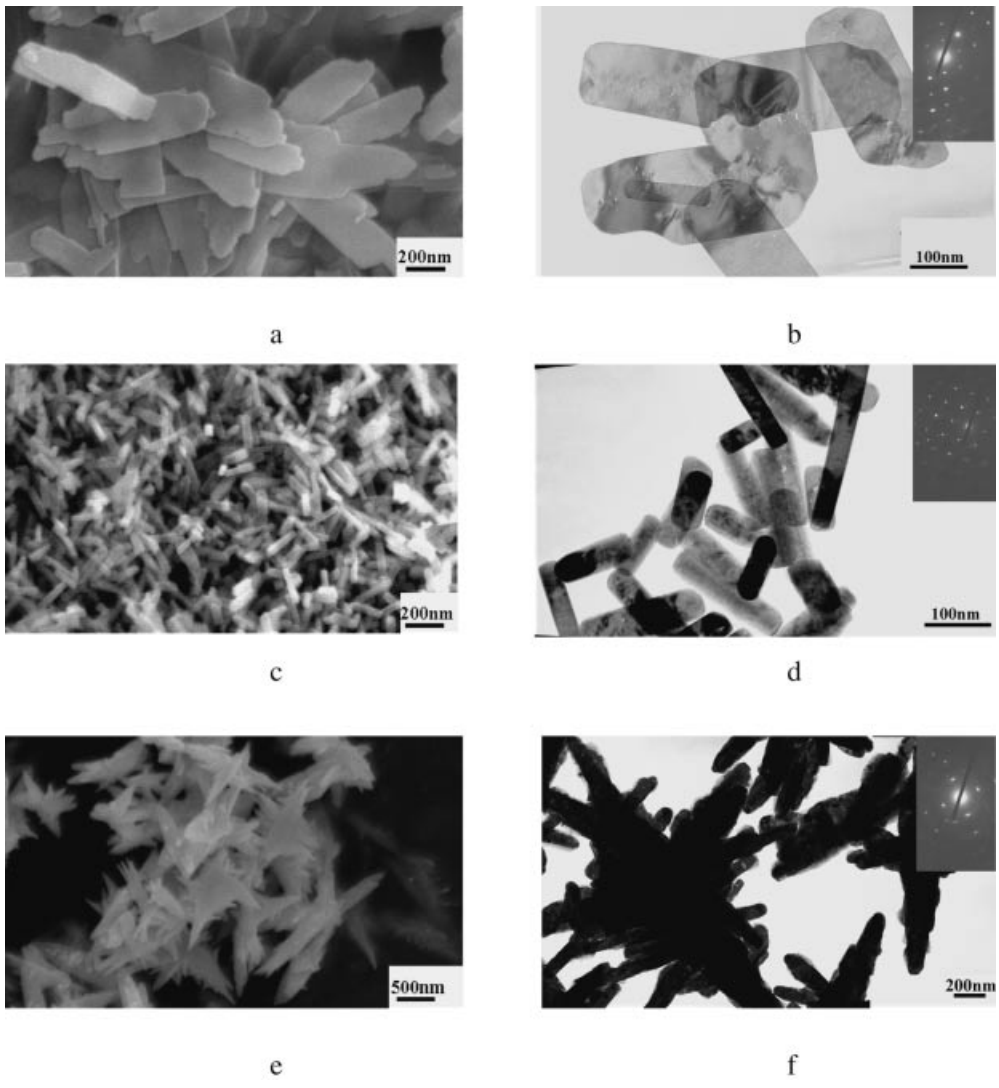

Figure 2. SEM images (a, c, e) and TEM images (b, d, f) of flakelike CuO (a and b, without sodium citrate), rodlike CuO (c and d, SC/Cu^{2+} = 1.0), and branchlike CuO (e and f, SC/Cu^{2+} = 1.3). The corresponding ED patterns of CuO are shown in the insets of the TEM images.

pH range 5–10 is the dimer $[Cu_2(cit)_2]^{4-}$ (cit^{4-} = $[C_6H_4O_7]^{4-}$).[36] When the SC/Cu^{2+} ratio is ≤1.0, the possible molecular structure of the citrate complex of Cu^{2+} (complex **1**) is shown in the Figure 3b. Two Cu^{2+} ions can form two six-membered rings and two seven-membered rings with two cit^{4-} ions. As the SC/Cu^{2+} ratio increases, the amount of complex **1** increases. Upon addition of NaOH solution, the formation of complex **1** delays the formation of $Cu(OH)_2$ nanoparticles and the crystal growth of $Cu(OH)_2$. Furthermore, the formation of complex **1** allows the elongation of the $Cu(OH)_2$ crystals in the direction perpendicular to the principal plane of the complex and elongation is inhibited in other directions. Therefore, the $Cu(OH)_2$ nanoparticles grow preferentially by the oriented attachment of the primary nanoparticles, which is coupled with coordination self-assembly thereby resulting in polycrystalline $Cu(OH)_2$ nanorods. With hydrothermal treatment the $Cu(OH)_2$ nanorods are transformed into CuO nanorods.

When the SC/Cu^{2+} ratio is more than 1.0, another citrate complex of Cu^{2+} (complex **2**, shown in the Figure 3c) appears. One Cu^{2+} ion forms two six-membered rings with two cit^{4-} ions. Strong H-bonds form between the carbonyl group ($-COO^-$) and the hydroxy group (–OH) in complex **2**. As the SC/Cu^{2+} ratio increases, the amount of complex **2** also increases. Upon adding NaOH solution, the H-bonds in complex **2** attacks the hydroxy ion in complex **1** that protrudes out of the edge of the orthorhombic $Cu(OH)_2$ with the corrugated layer structure. Consequently, the orthorhombic $Cu(OH)_2$ is activated, and the dehydrated reaction takes place more easily at the positions attacked by complex **2**. With hydrothermal treatment, the preferential growth of CuO occurs easily in the direction of attack by complex **2**, and branched CuO therefore forms. The XRD patterns of the branched CuO samples show that they are not pure monoclinic CuO samples – a weak peak of cubic Cu_2O also appears (Figure 1c). The appearance of the

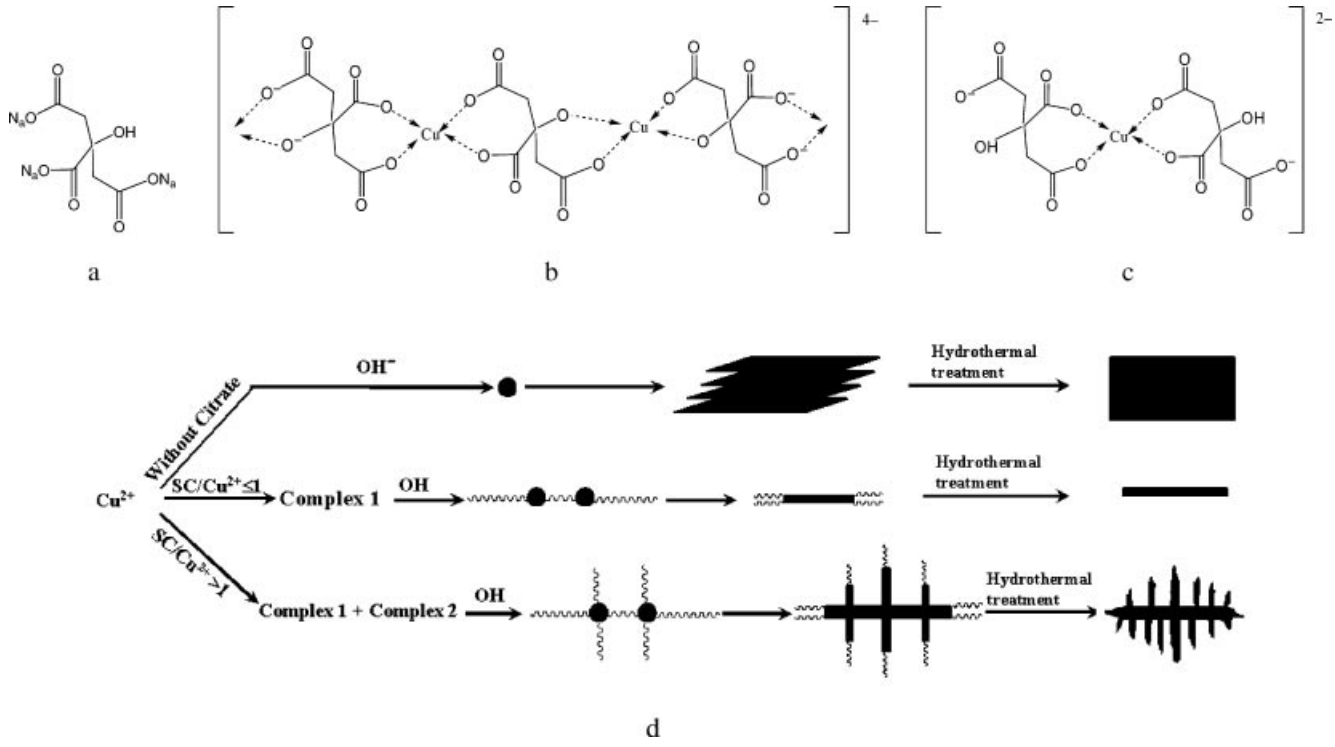

Figure 3. Molecular structures of (a) sodium citrate, (b) complex **1**, and (c) complex **2**, and (d) schematic illustration of the formation process for the as-prepared CuO nanostructures.

Cu_2O phase shows that citrate has a reducing capability. The above-mentioned results indicate that citrate, which acts as a modifying and reducing agent, plays a critical role in the determination of the morphology and in the control of the phase of the CuO nanostructures during the hydrothermal process. Yang et al. reported a similar result in the presence of ethylene glycol.[19]

A schematic diagram of the proposed growth mechanism is shown in Figure 3d. The formation of the flakelike CuO nanostructures without sodium citrate is determined by the internal crystallographic structure of the $Cu(OH)_2$ precursor.[28] After the addition of OH^-, orthorhombic $Cu(OH)_2$ first precipitates in solution. The orthorhombic $Cu(OH)_2$ consists of chains in the (001) planes, which are oriented along [100] and characterized by the square-planar coordination of the Cu^{2+} ions with strong H-bonds. By edge-sharing, a sheet of distorted $Cu(OH)_6$ octahedra is formed. The 2D layers of these sheets parallel to the (010) plane are connected through H-bonds. With hydrothermal treatment, orthorhombic $Cu(OH)_2$ transforms into flakelike, monoclinic CuO nanostructures by a dehydration reaction in which the interplanar H-bonds are broken. When the SC/Cu^{2+} ratio is ≤ 1.0, the formation of complex **1** leads to the formation of the rodlike CuO. When the SC/Cu^{2+} ratio is ≥ 1.0, the coexistence of complex **1** and complex **2** results in the appearance of branchlike CuO.

Optical Properties

The UV/Vis absorption spectrum of the CuO samples dispersed in distilled water (the concentration was about 0.02 $mgmL^{-1}$) is presented in Figure 4, which shows a broad absorption peak centered at about 335 nm. In principle, the optical bandgap energy for a semiconductor can be estimated by Equation (1),[37] where A is the absorbance, K is a constant, and m equals 1 for a direct transition.

$$A = \frac{K(hv - E_g)^{m/2}}{hv} \quad (1)$$

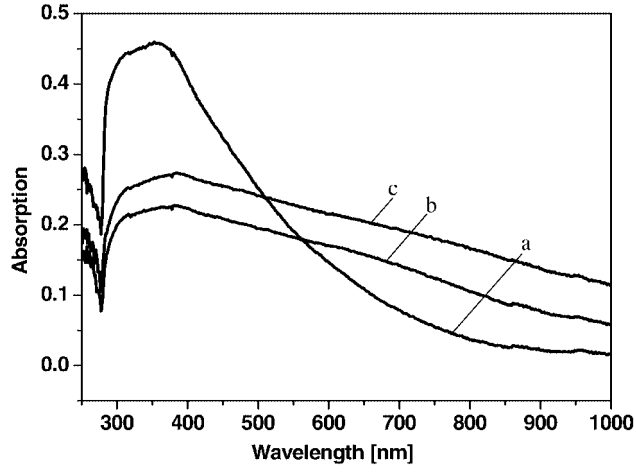

Figure 4. UV/Vis absorption spectrum of (a) rodlike CuO, (b) flakelike CuO, and (c) branchlike CuO.

Figure 5 shows a plot of $(A \cdot E_{phot})^2$ vs. photon energy (E_{phot}) for a direct transition. Extrapolation to $A = 0$ gives an absorption edge energy that corresponds to the bandgap energy E_g.[38] The bandgap energies of the 1D rodlike, 2D

flakelike, and 3D branchlike CuO samples were estimated to be 2.36, 1.60, and 1.40 eV, respectively, which are all larger than that reported for bulk CuO (E_g = 1.2 eV).[18d] The result shows that the bandgap of the CuO samples strongly depends on the morphology of the CuO products. A large enhancement of the bandgap energy of the CuO nanorods is attributed to the well-known quantum size effect for nanostructured semiconductors.[39] In addition, the different values of the bandgap energy of the CuO nanostructures with various morphologies indicates that the bandgap can be tuned by controlling the morphology of the CuO nanostructures.

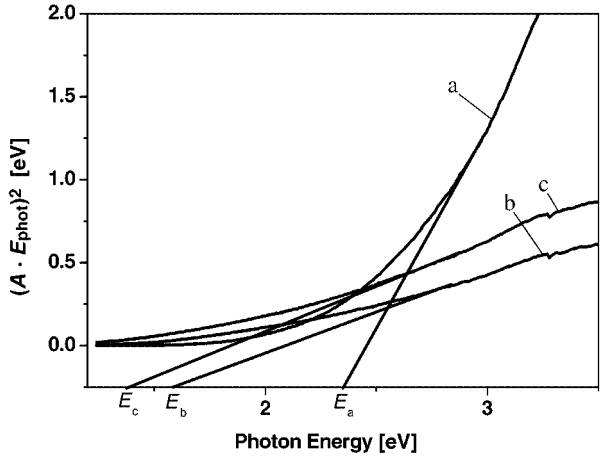

Figure 5. Plot of $(A \cdot E_{phot})^2$ vs. E_{phot} for a direct transition for (a) 1D rodlike CuO, (b) 2D flakelike CuO, and (c) 3D branchlike CuO.

Conclusions

The controlled synthesis of different nanostructured CuO samples has been achieved by a hydrothermal process in the presence of sodium citrate. It was found that the morphology of the CuO samples was affected by the SC/Cu^{2+} ratio. When the SC/Cu^{2+} ratio was below 1.0, 1D CuO nanorods with 30–40 nm diameters and 100–200 nm lengths were formed. In the absence of citrate, 2D flakelike CuO nanostructures were obtained. However, 3D branchlike CuO nanostructures were attained when the SC/Cu^{2+} ratio was more than 1.0. It is proposed that the formation of different nanostructured CuO is influenced by the different citrate complex of Cu^{2+} formed. The bandgap energies of the 1D rodlike, 2D flakelike, and 3D branchlike CuO nanostructures was estimated to be 2.36, 1.60, and 1.40 eV, respectively, which are all larger than that reported (E_g = 1.2 eV) for bulk CuO material.

Experimental Section

The chemical reagents including $CuSO_4 \cdot 5H_2O$, sodium citrate ($C_6H_5O_7Na_3 \cdot 2H_2O$), and sodium hydroxide were of analytical grade and used without further purification.

CuO nanostructures were synthesized by a hydrothermal process in the presence of sodium citrate. A typical synthesis of the CuO nanostructures is described as follows: $CuSO_4 \cdot 5H_2O$ (1.3 mmol) and a chosen amount of sodium citrate were dissolved in distilled water (40 mL), and the solution was constantly stirred for 15 min. NaOH (5.3 mmol) was then added to the above solution mixture. After 2.5 h of constant stirring, the final solution was transferred to a 50-mL Teflon-lined autoclave. The autoclave was then sealed in a stainless steel tank and kept at 160 °C for 12 h. The reactor was then naturally cooled to room temperature. The resulting samples were collected and washed with deionized water and dried at 50 °C in air. In order to investigate the influence of sodium citrate on the morphology of the final product, the molar ratio of sodium citrate to $CuSO_4 \cdot 5H_2O$ was changed from 0.1 to 1.5.

X-ray diffraction patterns [RINT 2000 Wilder-angel goniometer with Cu-K_α radiation (λ = 1.5406 Å)] and UV/Vis absorption spectra (Lambda 900 spectrometer) were used to characterize the as-obtained CuO nanostructures. The morphology of the CuO nanostructures was studied using transmission electron microscopy (Hitachi H-600 with an accelerating voltage of 200 kV) and scanning electron microscopy (Hitachi S-4300 microscope). The electron diffraction patterns were recorded with a JEOL JEM-2010 transmission electron microscope at an accelerating voltage of 200 kV.

Acknowledgments

Financial support of this work by the Overseas Outstanding Scholar Foundation of the Chinese Academy of Sciences (Grant Nos.: 2005–1-3 and 2005–2-1) and the National Natural Science Foundation of China (Grant No. 50573090) is gratefully acknowledged.

[1] M. K. Wu, J. R. Ashburn, C. J. Torng, P. H. Hor, R. L. Meng, L. Gao, Z. J. Huang, Y. Q. Wang, C. W. Chu, *Phys. Rev. Lett.* **1987**, *58*, 908–910.
[2] a) J. B. Reitz, E. I. Solomon, *J. Am. Chem. Soc.* **1998**, *120*, 11467–11478; b) K. B. Zhou, R. P. Wang, B. Q. Xu, Y. D. Li, *Nanotechnology* **2006**, *17*, 3939–3943.
[3] F. Lanza, R. Feduzi, J. Fuger, *J. Mater. Res.* **1990**, *5*, 1739–1744.
[4] M. Frietsch, F. Zudock, J. Goschnick, M. Bruns, *Sens. Actuators B* **2000**, *65*, 379–381.
[5] T. Maruyama, *Sol. Energy Mater. Sol. Cells* **1998**, *56*, 85–92.
[6] Y. Jiang, S. Decker, C. Mohs, K. J. Klabunde, *J. Catal.* **1998**, *180*, 24–35.
[7] B. Ao, L. Kummerl, K. Haarer, *Adv. Mater.* **1995**, *7*, 495–499.
[8] C. T. Hsieh, J. M. Chen, H. H. Lin, H. C. Shih, *Appl. Phys. Lett.* **2003**, *83*, 3383–3385.
[9] J. A. Switzer, H. M. Kothari, P. Poizot, S. Nakanishi, E. W. Bohannan, *Nature* **2003**, *425*, 490–493.
[10] A. Chowdhuri, V. Gupta, K. Sreenivas, R. Kumar, S. Mozumdar, P. K. Patanjali, *Appl. Phys. Lett.* **2004**, *84*, 1180–1182.
[11] X. P. Gao, J. L. Bao, G. L. Pan, H. Y. Zhu, P. X. Huang, F. Wu, D. Y. Song, *J. Phys. Chem. B* **2004**, *108*, 5547–5551.
[12] J. Chen, S. Deng, N. Xu, W. Zhang, X. Wen, S. Yang, *Appl. Phys. Lett.* **2003**, *83*, 746–748.
[13] P. Samarasekara, N. T. R. N. Kumara, N. U. S. Yapa, *J. Phys.: Condens. Mater.* **2006**, *18*, 2417–2420.
[14] J. T. Zhang, J. F. Liu, Q. Peng, X. Wang, Y. D. Li, *Chem. Mater.* **2006**, *18*, 867–871.
[15] a) Z. S. Hong, Y. Cao, J. F. Deng, *Mater. Lett.* **2002**, *52*, 34–38; b) S. H. Lee, Y. S. Her, E. Matijevic, *J. Colloid Interface Sci.* **1997**, *186*, 193–202; c) R. Yang, L. Gao, *Chem. Lett.* **2004**, *33*, 1194–1195; d) R. V. Kumar, R. Elgamiel, Y. Diamant, A. Gedanken, *Langmuir* **2001**, *17*, 1406–1410.
[16] a) D. Chen, G. Z. Shen, K. B. Tang, Y. T. Qian, *J. Cryst. Growth* **2003**, *254*, 225–228; b) Y. G. Zhang, S. T. Wang, X. B.

Li, L. Y. Chen, Y. T. Qian, Z. D. Zhang, *J. Cryst. Growth* **2006**, *291*, 196–201.
[17] a) C. K. Xu, Y. K. Liu, G. D. Xu, G. G. Wang, *Mater. Res. Bull.* **2002**, *37*, 2365–2372; b) D. Ghoshal, T. K. Maji, T. Mallah, T. H. Lu, G. Mostafa, N. R. Chaudhuri, *Inorg. Chim. Acta* **2005**, *358*, 1027–1033; c) T. Yu, F. C. Cheong, C. H. Sow, *Nanotechnology* **2004**, *15*, 1732–1736; d) W. Wang, Z. Liu, Y. Liu, C. Xu, C. Zheng, G. *Wang*, *Appl. Phys. A* **2003**, *76*, 417–420; e) C. H. Lo, T. T. Tsung, L. C. Chen, *J. Vac. Sci. Technol. B* **2005**, *23*, 2394–2397; f) Q. Liu, Y. Y. Liang, H. J. Liu, J. M. Hong, Z. Xu, *Mater. Chem. Phys.* **2006**, *98*, 519–522.
[18] a) Y. Chang, H. C. Zeng, *Cryst. Growth Des.* **2004**, *4*, 397–402; b) C. L. Zhu, C. N. Chen, L. Y. Hao, Y. Hu, Z. Y. Chen, *J. Cryst. Growth* **2004**, *263*, 473–479; c) C. L. Zhu, C. N. Chen, L. Y. Hao, Y. Hu, Z. Y. Chen, *Solid State Commun.* **2004**, *130*, 681–686; d) C. H. Lu, L. M. Qi, J. H. Yang, D. Y. Zhang, N. Z. Wu, J. M. Ma, *J. Phys. Chem. B* **2004**, *108*, 17825–17831; e) H. W. Hou, Y. Xie, Q. Li, *Cryst. Growth Des.* **2005**, *5*, 201–205.
[19] S. Z. Li, H. Zhang, Y. J. Ji, D. R. Yang, *Nanotechnology* **2004**, *15*, 1428–1432.
[20] a) Z. H. Liang, Y. J. Zhu, *Chem. Lett.* **2005**, *34*, 214–215; b) R. Yang, L. Gao, *Solid State Commun.* **2005**, *134*, 729–733; c) W. W. Wang, Y. J. Zhu, G. F. Cheng, Y. H. Huang, *Mater. Lett.* **2006**, *60*, 609–612; d) Q. Liu, H. J. Liu, Y. Y. Liang, Z. Xu, G. Yin, *Mater. Res. Bull.* **2006**, *41*, 697–702.
[21] a) X. Y. Song, S. X. Sun, W. M. Zhang, H. Y. Yu, W. L. Fan, *J. Phys. Chem. B* **2004**, *108*, 5200–5205; b) M. H. Cao, Y. H. Wang, C. X. Guo, Y. J. Qi, C. W. Hu, E. B. Wang, *J. Nanosci. Nanotechnol.* **2004**, *4*, 824–828; c) Y. D. Huh, S. S. Kweon, *Bulletin Korean Chem. Society* **2005**, *26*, 2054–2056.
[22] M. H. Cao, C. W. Hu, Y. H. Wang, Y. H. Guo, C. X. Guo, E. B. Wang, *Chem. Commun.* **2003**, *15*, 1884–1885.
[23] a) G. H. Du, G. V. Tendeloo, *Chem. Phys. Lett.* **2004**, *393*, 64–69; b) X. Y. Song, H. Y. Yu, S. X. Sun, *J. Colloid Interface. Sci.* **2005**, *289*, 588–591.
[24] Y. Y. Xu, D. R. Chen, X. L. Jiao, *J. Phys. Chem. B* **2005**, *109*, 13561–13566.
[25] L. Z. Zhang, J. C. Yu, A. W. Xu, Q. Li, K. W. Kwong, S. H. Yu, *J. Cryst. Growth* **2004**, *266*, 545–551.
[26] B. Liu, H. C. Zeng, *J. Am. Chem. Soc.* **2004**, *126*, 16744–16746.
[27] a) Z. H. Liang, Y. J. Zhu, *Chem. Lett.* **2004**, *33*, 1314–1315; b) G. F. Zou, H. Li, D. W. Zhang, K. Xiong, C. Dong, Y. T. Qian, *J. Phys. Chem. B* **2006**, *110*, 1632–1637.
[28] W. X. Zhang, X. G. Wen, S. H. Yang, *Inorg. Chem.* **2003**, *42*, 5005–5014.
[29] J. P. Liu, X. T. Huang, Y. Y. Li, K. M. Sulieman, X. He, F. L. Sun, *Cryst. Growth Des.* **2006**, *6*, 1690–1696.
[30] A. J. Heeger, *J. Phys. Chem. B* **2001**, *105*, 8475–8491.
[31] J. W. Zhu, H. Q. Chen, H. B. Liu, X. J. Yang, L. D. Lu, X. Wang, *Mater. Sci. Eng., A* **2004**, *384*, 172–176.
[32] H. H. Lin, C. Y. Wang, H. C. Shih, *J. Appl. Phys.* **2004**, *95*, 5889–5895.
[33] a) Z. S. Pillai, P. V. Kamat, *J. Phys. Chem. B* **2004**, *108*, 945–951; b) K. R. Brown, D. G. Walter, M. Natan, *Chem. Mater.* **2000**, *12*, 306–313; c) M. P. Mallin, C. Murphy, *Nano Lett.* **2002**, *2*, 1235–1237; d) G. J. Zhou, M. K. Lu, Z. S. Yang, H. P. Zhang, Y. Y. Zhou, S. M. Wang, S. F. Wang, A. Y. Zhang, *J. Cryst. Growth* **2006**, *289*, 255–259.
[34] a) M. Meyer, A. Bée, D. Talbot, V. Cabuil, J. M. Boyer, B. Répetti, R. Garrigos, *J. Colloid Interface Sci.* **2004**, *277*, 309–315; b) F. C. Meldrum, S. T. Hyde, *J. Cryst. Growth* **2001**, *231*, 544–558; c) Y. Wang, Z. Y. Tang, M. A. Correa-Duarte, I. Pastoriza-Santos, M. Giersig, N. A. Kotov, L. M. Liz-Marzan, *J. Phys. Chem. B* **2004**, *108*, 15461–15469; d) J. B. Liang, J. W. Liu, Q. Xie, S. Bai, W. C. Yu, Y. T. Qian, *J. Phys. Chem. B* **2005**, *109*, 9463–9467; e) Q. Y. Zhang, Y. Leng, H. J. Fan, J. Y. Chen, X. D. Zhang, *Key Eng. Mater.* **2006**, *309–311*, 387–390; f) L. P. Zhang, F. Guo, X. Z. Liu, *Mater. Res. Bull.* **2006**, *41*, 905–908.
[35] Joint Committee on Powder Diffraction Standards. Diffraction Data File No. 5–661; JCPDS International Center for Diffraction Data, Pennsylvania, **1991**.
[36] P. G. Daniele, G. Ostacoli, O. Zerbinati, S. Sammartano, *Transition Met. Chem.* **1988**, *13*, 87–91.
[37] B. Subramanian, C. Sanjeeviraja, M. Jayachandran, *J. Cryst. Growth* **2002**, *234*, 421–426.
[38] S. Tsunekawa, T. Fukuda, A. Kasuya, *J. Appl. Phys.* **2000**, *87*, 1318–1321.
[39] J. P. Yang, F. C. Meldrum, J. H. Fendler, *J. Phys. Chem.* **1995**, *99*, 5500–5504.

Received: November 2, 2006
Published Online: March 30, 2007

